7028 *Inorg. Chem.* **2010**, *49*, 7028–7034
DOI: 10.1021/ic100706n

Inorganic Chemistry
Article

New Noncentrosymmetric Tellurite Phosphate Material: Synthesis, Characterization, and Calculations of $Te_2O(PO_4)_2$

Min Kyung Kim,[†] Sang-Hwan Kim,[‡] Hong-Young Chang,[‡] P. Shiv Halasyamani,[‡] and Kang Min Ok*[,†]

[†] *Department of Chemistry, Chung-Ang University, 221 Heukseok-dong, Dongjak-gu, Seoul 156-756, Republic of Korea, and* [‡] *Department of Chemistry, University of Houston, 136 Fleming Building, Houston, Texas 77204-5003*

Received April 13, 2010

A new noncentrosymmetric polar ternary tellurium(IV) oxide phosphate, $Te_2O(PO_4)_2$, has been synthesized by a standard solid-state reaction, and the structure was determined by single crystal X-ray diffraction. The material shows a three-dimensional framework structure that is composed of slightly distorted TeO_5 square pyramids and PO_4 tetrahedra. Within the framework three-, four-, and seven-membered ring channels are observed along the [100] direction. In addition to structural characterization, second-harmonic generation (SHG) and piezoelectric measurements were performed. Powder SHG measurement on the $Te_2O(PO_4)_2$, using 1064 nm radiation, indicated the material has a SHG efficiency of approximately $50 \times \alpha\text{-SiO}_2$. Converse piezoelectric measurements revealed a d_{33} value of 20 pm V^{-1}. Thermogravimetric analysis, UV−vis diffuse reflectance, and infrared spectroscopy were also performed, as were electronic structure calculations. Crystal data: $Te_2O(PO_4)_2$, monoclinic, space group *Cc* (No. 9), with $a = 5.3819(7)$ Å, $b = 13.6990(19)$ Å, $c = 9.5866(12)$ Å, $V = 686.73(16)$ Å^3, and $Z = 4$.

Introduction

Tellurium(IV) oxide phosphate materials have received significant attention for their rich structural chemistry attributable to the composing building blocks, that is, TeO_x (x = 4 or 5) and PO_4 groups.[1−7] While the TeO_x group normally exhibits variable coordination environments such as trigonal pyramid, seesaw, square pyramid, and so forth, the PO_4 group shows a tetrahedral geometry. From the various coordination geometries and their combination subsequently result in the formation of a wide variety of structural topologies. Further, tellurium(IV) oxide materials, that is, tellurites, also possess asymmetric structural geometry owing to the nonbonded electron pair on the Te^{4+} cation.[8−11] Materials containing lone pair cations such as Te^{4+} have proven to easily crystallize in noncentrosymmetric (NCS) crystal structures attributable to their local acentric coordination environments.[12−16] Regardless of the dimensions of the materials, a number of strategies have been suggested to increase the incidence of crystallographic NCS structures in any new material,[17−22] since they could reveal extremely important technological properties such as second harmonic generation (SHG), piezoelectricity, ferroelectricity,

---

*To whom correspondence should be addressed. E-mail: kmok@cau.ac.kr. Phone: +82-2-820-5197. Fax: +82-2-825-4736.

(1) Mayer, H. Z. *Kristallogr. Kristallgeom. Kristallphys. Kristallchem.* **1975**, *141*, 354.

(2) Mayer, H.; Pupp, G. Z. *Kristallogr. Kristallgeom. Kristallphys. Kristallchem.* **1977**, *145*, 321.

(3) Alcock, N. W.; Harrison, W. D. *Acta Crystallogr.* **1982**, *B38*, 1809.

(4) Guesdon, A.; Raveau, B. *Chem. Mater.* **2000**, *12*, 2239.

(5) Mayer, H.; Weil, M. *Z. Anorg. Allg. Chem.* **2003**, *629*, 1068.

(6) Ok, K. M.; Orzechowski, J.; Halasyamani, P. S. *Inorg. Chem.* **2004**, *43*, 964.

(7) Ok, K. M.; Halasyamani, P. S. *J. Solid State Chem.* **2006**, *179*, 1345.

(8) Arnaud, Y.; Averbuch-Pouchot, M. T.; Durif, A.; Guidot, J. *Acta Crystallogr.* **1976**, *B32*, 1417.

(9) Alonso, J. A.; Castro, A.; Gutierrez-Puebla, E.; Monge, M. A.; Rasines, I.; Ruiz-Valero, C. *J. Solid State Chem.* **1987**, *69*, 36.

(10) Zid, M. F.; Jouini, T.; Jouini, N. *C.R. Acad. Sci. Ser. IIc: Chim.* **1989**, *309*, 343.

(11) Balraj, V.; Vidyasagar, K. *Inorg. Chem.* **1998**, *37*, 4764.

(12) Halasyamani, P. S.; Poeppelmeier, K. R. *Chem. Mater.* **1998**, *10*, 2753.

(13) Ok, K. M.; Bhuvanesh, N. S. P.; Halasyamani, P. S. *Inorg. Chem.* **2001**, *40*, 1978.

(14) Ra, H.-S.; Ok, K. M.; Halasyamani, P. S. *J. Am .Chem. Soc.* **2003**, *125*, 7764.

(15) Ok, K. M.; Halasyamani, P. S. *Angew. Chem., Int. Ed.* **2004**, *43*, 5489.

(16) Ok, K. M.; Halasyamani, P. S. *Inorg. Chem.* **2005**, *44*, 9353.

(17) Bruce, D.; Wilkinson, A. P.; While, M. G.; Bertrand, J. A. *J. Solid State Chem.* **1996**, *125*, 228.

(18) Kepert, C. J.; Prior, T. J.; Rosseinsky, M. J. *J. Am. Chem. Soc.* **2000**, *122*, 5158.

(19) Maggard, P. A.; Stern, C. L.; Poeppelmeier, K. R. *J. Am. Chem. Soc.* **2001**, *123*, 7742.

(20) Evans, O. R.; Lin, W. *Acc. Chem. Res.* **2002**, *35*, 511.

(21) Hwu, S.-J.; Ulutagay-Kartin, M.; Clayhold, J. A.; Mackay, R.; Wardojo, T. A.; O'Connor, C. J.; Kraweic, M. *J. Am. Chem. Soc.* **2002**, *124*, 12404.

(22) Welk, M. E.; Norquist, A. J.; Arnold, F. P.; Stern, C. L.; Poeppelmeier, K. R. *Inorg. Chem.* **2002**, *41*, 5119.

and pyroelectricity.[23−26] With oxide materials, the NCS structures are often observed from the two inherently asymmetric second-order Jahn−Teller (SOJT) distortive cations:[27−32] octahedrally coordinated d^0 transition-metal ions (Ti^{4+}, V^{5+}, Mo^{6+}, etc.) and lone-pair cations (Sb^{3+}, Te^{4+}, I^{5+}, etc.). While an out-of-center displacement toward a corner, edge, or face of the octahedron attributable to mixing between the empty metal d- and filled oxygen p-orbitals is responsible for the asymmetric geometry of the d^0 metal ions,[33] nonbonded electron pairs involving metal s-p mixing as well as oxygen 2p orbitals are found from the lone pair cations.[34−36] Because the asymmetric environments are one of the dominant factors that influence the materials' NCS properties, to understand the structural basis of the local asymmetric environments is very important. However, the local asymmetric environment is a necessary, but not sufficient condition for creating macroscopic NCS structures. In other words, once the local acentric units are aligned in an antiparallel manner, the material may crystallize in a centrosymmetric structure. Thus, understanding the factors that determine macroscopic centricity is as much important as understanding the local asymmetry, and the rational design of NCS materials still remains an ongoing challenge. In this paper, we report on the solid-state synthesis, structure, and characterization of a new polar ternary tellurium(IV) oxide phosphate, $Te_2O(PO_4)_2$. Although several tellurium(IV) oxide phosphate materials such as $Te_2O_3(HPO_4)$,[1,3] $Te_8O_{10}(PO_4)_4$,[2] $A_2TeMo_2O_6(PO_4)_2$ (A = K, Rb, Tl, Cs),[4] $Te_3O_3(PO_4)_2$,[5] $BaTeMO_4(PO_4)$,[6] and $Ba_2TeO(PO_4)_2$[7] have been reported, only $Te_2O_3(HPO_4)$ crystallizes in NCS structure. Besides, no NCS properties has been reported for any tellurium(IV) oxide phosphate material yet. Thus, we are going to explore the detailed NCS materials' properties for $Te_2O(PO_4)_2$. As such, SHG and piezoelectricity on $Te_2O(PO_4)_2$ were performed. We also performed thermogravimetric analysis, UV−vis diffuse reflectance, infrared spectroscopy, and electronic structure calculations.

Experimental Section

Reagents. TeO_2 (Alfa Aesar, 99.9%), $(NH_4)H_2PO_4$ (Aldrich, ≥98.5%), and P_4O_{10} (Aldrich, 98+%) were used as received.

Synthesis. Crystals of $Te_2O(PO_4)_2$ were prepared by using TeO_2 and P_4O_{10}. A 0.112 g portion (7.00×10^{-4} mol) of TeO_2 and 0.100 g (3.50×10^{-4} mol) of P_4O_{10} were thoroughly mixed with an agate mortar and pestle under an atmosphere of dry argon and pressed into a pellet. The pellet was introduced into a fused silica tube that was evacuated and subsequently sealed. The tube was gradually heated to 550 °C, held for 24 h, and cooled to room temperature at a rate of 6 °C h^{-1}. The powder X-ray diffraction pattern on the resultant colorless block crystals indicated the material was single-phase. Alternatively, pure polycrystalline samples of $Te_2O(PO_4)_2$ were obtained from the solid-state reaction of TeO_2 and $(NH_4)H_2PO_4$. A 0.463 g portion (2.90×10^{-3} mol) of TeO_2 and 0.334 g (2.90×10^{-3} mol) of $(NH_4)H_2PO_4$ were thoroughly mixed, pelletized, heated at 210 °C for 12 h. The product was reground, pelletized, and heated to 500 °C for 12 h in air and cooled down to the room temperature at a rate of 5 °C min^{-1}. Powder X-ray diffraction on the resultant polycrystalline sample was in a good agreement with the generated pattern from the single-crystal structure.

Table 1. Crystallographic Data for $Te_2O(PO_4)_2$

formula	$Te_2P_2O_9$	T (°C)	298.0(2)
formula weight	461.14	λ (Å)	0.71073
crystal dimensions (mm^3)	$0.08 \times 0.20 \times 0.30$	ρ_{calcd} (g cm^{-3})	4.460
color, habit	colorless block	μ (mm^{-1})	8.989
crystal system	monoclinic	$2\theta_{max}$ (deg)	55.62
space group	*Cc* (No. 9)	reflection collected/unique	2031/1026
a (Å)	5.3819(7)	absorption correction	SADABS
b (Å)	13.6990(19)	R(int)	0.0393
c (Å)	9.5866(12)	GOF	1.046
β (deg)	103.682(2)	extinction coefficient	0.054(2)
V (Å^3)	686.73(16)	$R(F)^a$	0.0307
Z	4	$R_w(F_o^2)^b$	0.0854

$^aR(F) = \sum||F_o| - |F_c||/\sum|F_o|$. $^bR_w(F_o^2) = [\sum w(F_o^2 - F_c^2)^2/\sum w(F_o^2)^2]^{1/2}$.

Single Crystal X-ray Diffraction. The structure of $Te_2O(PO_4)_2$ was determined by standard crystallographic methods. A colorless block ($0.08 \times 0.20 \times 0.30$ mm^3) was used for single crystal data analysis. All of the data were collected using a Bruker SMART APEX diffractometer equipped with a 1K CCD area detector using graphite monochromated Mo Kα radiation at room temperature at the Korea Basic Science Institute. A hemisphere of data was collected using a narrow-frame method with scan widths of 0.30° in ω, and an exposure time of 5 s/frame. The first 50 frames were remeasured at the end of the data collection to monitor instrument and crystal stability. The maximum correction applied to the intensities was < 1%. The data were integrated using the SAINT program,[37] with the intensities corrected for Lorentz, polarization, air absorption, and absorption attributable to the variation in the path length through the detector faceplate. A semiempirical absorption correction was made on the hemisphere of data with the SADABS program.[38] The data were solved and refined using SHELXS-97 and SHELXL-97, respectively.[39,40] All of the atoms were refined with anisotropic thermal parameters and converged for $I > 2\sigma(I)$. All calculations were performed using the WinGX-98 crystallographic software package.[41] Crystallographic data and selected bond distances for the reported material are given in Tables 1 and 2.

Powder X-ray Diffraction (XRD). Powder XRD was used to confirm the phase purity for the synthesized material. The XRD data were collected on a Scintag XDS2000 diffractometer at room temperature (Cu Kα radiation, $\theta-\theta$ mode, flat plate geometry) equipped with Peltier germanium solid state detector in the 2θ range 5−70° with a step size of 0.02°, and a step time of

---

(23) Jona, F.; Shirane, G. *Ferroelectric Crystals*; Pergamon Press: Oxford, 1962.

(24) Cady, W. G. *Piezoelectricity; an Introduction to the Theory and Applications of Electromechanical Phenomena in Crystals*; Dover: New York, 1964; p 822.

(25) Lang, S. B. *Sourcebook of Pyroelectricity*; Gordon & Breach Science: London, 1974.

(26) Galy, J.; Meunier, G. *J. Solid State Chem.* **1975**, *13*, 142.

(27) Opik, U.; Pryce, M. H. L. *Proc. R. Soc. London* **1957**, *A238*, 425.

(28) Bader, R. F. W. *Mol. Phys.* **1960**, *3*, 137.

(29) Bader, R. F. W. *Can. J. Chem.* **1962**, *40*, 1164.

(30) Pearson, R. G. *J. Am. Chem. Soc.* **1969**, *91*, 4947.

(31) Pearson, R. G. *J. Mol. Struct.: THEOCHEM* **1983**, *103*, 25.

(32) Wheeler, R. A.; Whangbo, M.-H.; Hughbanks, T.; Hoffmann, R.; Burdett, J. K.; Albright, T. A. *J. Am. Chem. Soc.* **1986**, *108*, 2222.

(33) Goodenough, J. B. *Annu. Rev. Mater. Sci.* **1998**, *28*, 1.

(34) Orgel, L. E. *J. Chem. Soc.* **1959**, 3815.

(35) Waghmare, U. V.; Spaldin, N. A.; Kandpal, H. C.; Seshadri, R. *Phys. Rev. B* **2003**, *67*, 12511–1.

(36) Stoltzfus, M. W.; Woodward, P.; Seshadri, R.; Park, J.-H.; Bursten, B. *Inorg. Chem.* **2007**, *46*, 3839.

(37) *SAINT, Program for Area Detector Absorption Correction*, version 4.05; Siemens Analytical X-ray Instruments: Madison, WI, 1995.

(38) Blessing, R. H. *Acta Crystallogr.* **1995**, *A51*, 33.

(39) Sheldrick, G. M. *SHELXS-97 - A program for automatic solution of crystal structures*; University of Goettingen: Goettingen, Germany, 1997.

(40) Sheldrick, G. M. *SHELXL-97 - A program for crystal structure refinement*; University of Goettingen: Goettingen, Germany: 1997.

(41) Farrugia, L. J. *J. Appl. Crystallogr.* **1999**, *32*, 837.

Table 2. Selected Bond Distances (Å) for $Te_2O(PO_4)_2$

Te(1)−O(1)	2.130(9)	P(1)−O(1)	1.537(7)
Te(1)−O(2)	2.230(10)	P(1)−O(4)	1.560(8)
Te(1)−O(3)	2.046(9)	P(1)−O(7)	1.559(9)
Te(1)−O(4)	2.118(9)	P(1)−O(8)	1.548(9)
Te(1)−O(5)	1.910(8)	P(2)−O(2)	1.559(8)
Te(2)−O(5)	1.917(8)	P(2)−O(3)	1.536(10)
Te(2)−O(6)	2.104(9)	P(2)−O(6)	1.555(10)
Te(2)−O(7)	2.074(8)	P(2)−O(9)	1.558(9)
Te(2)−O(8)	2.070(10)		
Te(2)−O(9)	2.123(9)		

1 s. The experimental powder XRD pattern is in good agreement with the calculated data from the single-crystal model.

Infrared Spectroscopy. Infrared spectrum was recorded on a Varian 1000 FT-IR spectrometer in the 400−4000 cm^{-1} range, with the sample pressed between two KBr pellets.

UV−vis Diffuse Reflectance Spectroscopy. UV−visible reflectance data were collected on a Varian Cary 500 scan UV−vis-NIR spectrophotometer over the spectral range 200−1500 nm at room temperature. Poly(tetrafluoroethylene) was used as a reference material. Reflectance spectrum was converted to the absorbance using the Kubelka−Munk function.[42,43]

Thermogravimetric Analysis. Thermogravimetric analysis was performed on a Setaram LABSYS TG-DTA/DSC Thermogravimetric Analyzer. The polycrystalline $Te_2O(PO_4)_2$ sample was contained within an alumina crucible and heated at a rate of 10 °C min^{-1} from room temperature to 800 °C under flowing argon.

Second-Order Nonlinear Optical Measurements. Powder SHG measurements on polycrystalline $Te_2O(PO_4)_2$ were performed on a modified Kurtz-NLO system[44] using 1064 nm radiation. A detailed description of the equipment and the methodology used has been published.[45] SHG efficiency has been shown to depend strongly on particle size, thus polycrystalline samples were ground and sieved into distinct particle size ranges (20−45, 45−63, 63−75, 75−90, >90 μm). To make relevant comparisons with known SHG materials, crystalline α-SiO_2 and $LiNbO_3$ were also ground and sieved into the same particle size ranges. Powders with particle size 45−63 μm were used for comparing SHG intensities. No index matching fluid was used in any of the experiments.

Piezoelectric Measurements. Piezoelectric measurements were performed using a Radiant Technologies RT66A piezoelectric test system with a TREK (model $609E^{-6}$) high voltage amplifier, Precision Materials Analyzer, Precision High Voltage Interface, and MTI 2000 Fotonic Sensor. The polycrystalline $Te_2O(PO_4)_2$ was pressed into a 13 mm diameter and ~1.2 mm thick pellet. The pellet was annealed at 650 °C for 12 h. A conducting silver paste was applied to both sides of the pellet surfaces for electrodes. A maximum voltage of 500 V was applied to the sample. Twenty measurements were performed and an average was taken.

Electronic Structure Calculations. First principles electronic band structure calculations were performed utilizing the plane wave pseudopotential (PWPP)[46] and tight-binding linear muffin-tin orbital (TB-LMTO) methods[47,48] based upon density functional theory (DFT). For the PWPP calculations, the Quantum ESPRESSO (4.0.1 version) package[49] was employed. Norm-conserving Martins-Troullier pseudopotentials (MTPPs) for all the elements were used with the generalized gradient approximation (GGA)[50] for the exchange-correlation corrections. A plane wave energy cutoff was set to 37 Ry. A Gaussian smearing of 0.01 Ry for Brillouin zone integrations was adopted with a 9 × 3 × 5 k-point mesh in the *C*-centered monoclinic unit cell. TB-LMTO calculations were performed within the atomic sphere approximation (ASA). The von Barth-Hedin local exchange-correlation potential[51] was utilized for the local density approximation (LDA). The radial scalar relativistic Dirac equation was solved for obtaining the partial waves. A total of 20 empty spheres introduced were necessary to attain space filling for $Te_2O(PO_4)_2$. A total of 84 irreducible k-points from 6 × 6 × 4 grid was used for Brillouin zone integrations by tetrahedron method.[46,52,53] The basis set consisted of Te-5s/5p/[5d]/[4f], P-3s/3p/[3d], and O-2s/2p/[3s]/[3d] orbitals where the orbital in bracket was treated with the downfolding technique.[54] Total energy changes of less than 10^{-5} Ry indicated self-consistency.

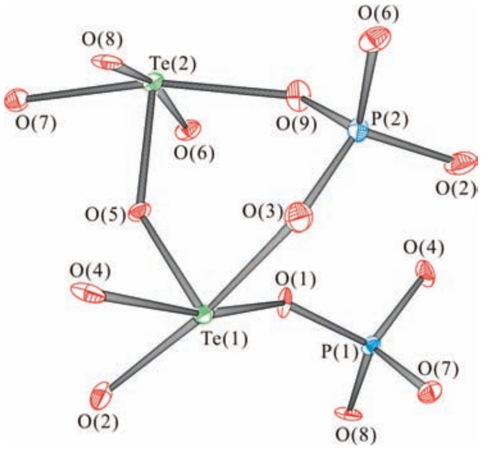

Figure 1. ORTEP (50% probability ellipsoids) drawing for $Te_2O(PO_4)_2$.

Results and Discussion

Structure. $Te_2O(PO_4)_2$ is a new ternary tellurium(IV) oxide phosphate material crystallizing in a NCS polar space group *Cc*. The structure contains PO_4 tetrahedra and asymmetric TeO_5 polyhedra, which are connected by Te−O−Te and Te−O−P bonds (see Figure 1). However, no P−O−P bond is observed within the structure. There are two unique Te^{4+} cations that are in distorted square pyramidal environment, bonded to five oxygen atoms. The Te−O bond lengths range from 1.910(8) to 2.230(10) Å. A list of the selected bond distances is given in Table 2. The bond distances are consistent with those previously reported.[1−7] The O−Te−O bond angles range from 80.6(3) to 173.2(3)°. The Te^{4+} cations are in a highly asymmetric coordination environment attributed to their nonbonded electron pair. The two unique P^{5+} cations are in slightly distorted tetrahedral geometry, linked to four oxygen atoms. The P−O bond distances range from 1.536(10) to 1.560(8) Å. The O−P−O bond angles range from 107.6(5) to 111.9(5)°. Each oxygen atom is bonded

---

(42) Kubelka, P.; Munk, F. *Z. Tech. Phys.* **1931**, *12*, 593.
(43) Tauc, J. *Mater. Res. Bull.* **1970**, *5*, 721.
(44) Kurtz, S. K.; Perry, T. T. *J. Appl. Phys.* **1968**, *39*, 3798.
(45) Ok, K. M.; Chi, E. O.; Halasyamani, P. S. *Chem. Soc. Rev.* **2006**, *35*, 710.
(46) Pickett, W. E. *Comput. Phys. Rep.* **1989**, *9*, 115.
(47) Andersen, O. K. *Phys. Rev. B* **1975**, *12*, 3060.
(48) Andersen, O. K.; Jepsen, O. *Phys. Rev. Lett.* **1984**, *53*, 2571.
(49) Baroni, S.; Dal Corso, A.; de Gironcoli, S.; Giannozzi, P.; Cavazzoni, C.; Ballabio, G.; Scandolo, S.; Chiarotti, G.; Focher, P.; Pasquarello, A.; Laasonen, K.; Trave, A.; Car, R.; Marzari, N.; Kokalj, A. http://www.quantum-espresso.org/.
(50) Perdew, J. P.; Burke, K.; Ernzerhof, M. *Phys. Rev. Lett.* **1996**, *77*, 3865.
(51) Von Barth, U.; Hedin, L. *J. Phys. C: Solid State Phys.* **1972**, *5*, 1629.
(52) Jepsen, O.; Andersen, O. K. *Solid State Commun.* **1971**, *9*, 1763.
(53) Jepsen, O.; Andersen, O. K. *Phy. Rev. B* **1984**, *29*, 5965.
(54) Lambrecht, W. R. L.; Andersen, O. K. *Phys. Rev. B: Condens. Matter* **1986**, *34*, 2439.

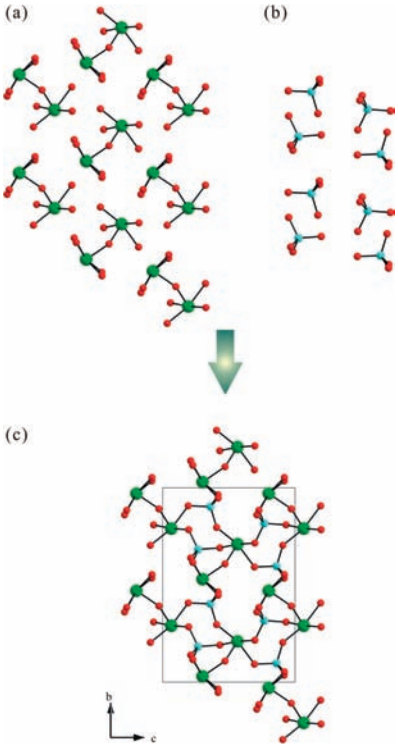

Figure 2. Ball-and-stick diagrams of (a) Te_2O_9 dimers, (b) PO_4 tetrahedra, and (c) the "linking" of the Te_2O_9 dimers by PO_4 tetrahedra to form a framework of $Te_2O(PO_4)_2$ (green, Te; cyan, P; red, O).

to two atoms; while the O(5) is linked to two Te^{4+} cations, all the other oxygen atoms are coordinated to both Te^{4+} and P^{5+} cations. Thus, in connectivity terms, the structure may be written as a neutral framework of $\{[Te(1)O_{5/2}]^- [Te(2)O_{5/2}]^- [P(1)O_{4/2}]^+ [P(2)O_{4/2}]^+\}^0$. Bond valence calculations[55,56] on $Te_2O(PO_4)_2$ resulted in values of 4.00−4.11 and 4.81−4.83 for Te^{4+} and P^{5+}, respectively. The two five-coordinate $Te(1)O_5$ and $Te(2)O_5$ square pyramids are sharing their corner through O(5) and are forming a Te_2O_9 "dimer" (see Figure 2a). Each Te_2O_9 dimer is connected by PO_4 tetrahedra through O(1), O(2), O(3), O(4), O(6), O(7), O(8), and O(9) and forms a novel three-dimensional framework (see Figure 2). Interestingly, three-, four-, and seven-membered ring channels are observed along the [100] direction in the framework structure (see Figure 3). The dimension of the seven-membered ring is approximately 1.7 Å × 5.3 Å, taking into account the atomic radii of oxygen.[57]

Infrared Spectroscopy. The infrared spectrum of $Te_2O(PO_4)_2$ exhibits Te−O, P−O, and Te−O−P vibrations. The Te−O vibrations are observed around 628−773 and 416 cm^{-1}. The bands occurring about 975−1121 and 451−577 cm^{-1} can be assigned to P−O vibrations. A band occurring around 606 cm^{-1} is attributed to Te−O−P vibration. The infrared vibrations and assignments are listed in Table 3. The assignments are consistent with those previously reported.[58,59]

UV−vis Diffuse Reflectance Spectroscopy. $Te_2O(PO_4)_2$ is white and the UV−vis diffuse reflectance spectrum shows that it is transparent. Absorption (K/S) data were calculated from the following Kubelka−Munk function:[42,43]

$$F(R) = \frac{(1-R)^2}{2R} = \frac{K}{S}$$

where R is the reflectance, K the absorption, and S the scattering. In the (K/S)-versus-E plot, extrapolating the linear part of the rising curve to zero provided the onset of absorption at ~4 eV for $Te_2O(PO_4)_2$. The band gap is mainly attributable to the degree of the distortions arising from TeO_5 and PO_4 groups. The UV−vis diffuse reflectance spectrum is deposited in the Supporting Information.

Thermogravimetric Analysis. $Te_2O(PO_4)_2$ is stable up to 800 °C, as indicated by the thermogravimetric analysis diagram. No weight change has been observed. The TGA plot for $Te_2O(PO_4)_2$ is shown in the Supporting Information.

Second Harmonic Generation. As $Te_2O(PO_4)_2$ crystallizes in NCS space group *Cc*, we investigated its SHG properties. Powder SHG measurements, using 1064 nm radiation, indicated that $Te_2O(PO_4)_2$ has a SHG efficiency of approximately 50 × α-SiO_2. By sieving $Te_2O(PO_4)_2$ into various particle sizes, ranging from 20−150 μm, and measuring the SHG as a function of particle size, we were able to determine the Type 1 phase-matching capabilities of the material. We determined that $Te_2O(PO_4)_2$ is not phase-matchable (see the Supporting Information). On the basis of the SHG efficiency and phase-matching measurements, $Te_2O(PO_4)_2$ falls into the class C category of SHG materials, as defined by Kurtz and Perry.[44] Once the SHG efficiency has been measured and the phase-matching behavior determined, the bulk SHG efficiency, $\langle d_{eff} \rangle_{exp}$, can be estimated.[60] For $Te_2O(PO_4)_2$, $\langle d_{eff} \rangle_{exp}$ is approximately 3.9 pm V^{-1}.

Piezoelectric Measurement. Space group *Cc* exhibits the correct symmetry for SHG as well as piezoelectricity. Thus, converse piezoelectric measurements were performed on $Te_2O(PO_4)_2$. In this measurement, the application of a voltage results in the macroscopic deformation of the material, which in turn is occurring as a strain parallel to the direction of the polarization. A maximum voltage of 500 V was applied to the sample. Twenty measurements were performed, and an average was taken. The graph of the piezoelectric data has been deposited in the Supporting Information. The piezoelectric charge constant, d_{33}, was calculated from

$$\Delta L = S \times L_0 \sim E \times d_{33} \times L_0$$

where ΔL is the displacement of the sample, L_0 is the sample thickness (m), S is the strain ($\Delta L/L_0$), and E is the electric field strength (V m^{-1}). We estimate d_{33} values of 20 pm V^{-1} for $Te_2O(PO_4)_2$. The value is similar to that of $LiNbO_3$ (d_{33} = 6−19 pm V^{-1}).[61]

Electronic Structure Analysis. As mentioned earlier, calculations of the electronic energy band structures of

---

(55) Brown, I. D.; Altermatt, D. *Acta Crystallogr.* **1985**, *B41*, 244.

(56) Brese, N. E.; O'Keeffe, M. *Acta Crystallogr.* **1991**, *B47*, 192.

(57) Shannon, R. D. *Acta Crystallogr.* **1976**, *A32*, 751.

(58) Belik, A. A.; Izumi, F.; Azuma, M.; Kamiyama, T.; Oikawa, K.; Pokholok, K. V.; Lazoryak, B. I.; Takano, M. *Chem. Mater.* **2005**, *17*, 5455.

(59) Tomaszewski, P. E.; Maczka, M.; Majchrowski, A.; Waskowska, A.; Hanuza, J. *Solid State Sci.* **2005**, *7*, 1201.

(60) Goodey, J.; Broussard, J.; Halasyamani, P. S. *Chem. Mater.* **2002**, *14*, 3174.

(61) Landolt, H. *Numerical Values and Functions from the Natural Sciences and Technology* (*New Series*), *Group 3: Crystal and Solid State Physics*; Springer Verlag: Berlin, 1979; Vol. *11*, p 317 ff.

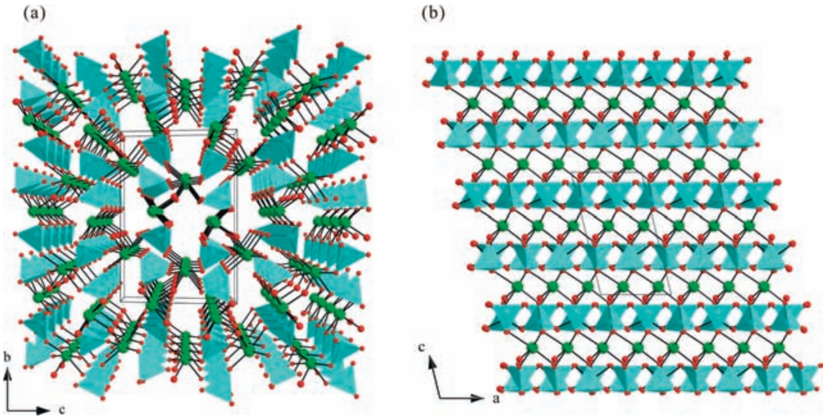

Figure 3. Ball-and-stick and polyhedral representations of $Te_2O(PO_4)_2$ (a) in the *bc*-plane and (b) *ac*-plane (green, Te; cyan, P; red, O). Three-, four-, and seven-membered ring channels are observed along the [100] direction.

Table 3. Infrared Vibrations (cm^{-1}) for $Te_2O(PO_4)_2$

P−O	Te−O	P−O−Te
1121	773	606
1004	628	
975	416	
577		
524		
451		

$Te_2O(PO_4)_2$ were carried out using the pseudopotential and TB-LMTO-ASA methods. Similar electronic energy band structures for $Te_2O(PO_4)_2$ were calculated from both methods. Figure 4 shows the total and projected density of states (DOSs) calculated from the pseudopotential method. The electronic structure shows an approximate energy gap of 2.1 eV at the Fermi level (E_F) for $Te_2O(PO_4)_2$ that is considerably smaller than the experimentally observed energy gap of 4 eV in the UV−vis diffuse reflective spectrum. The tendency for electronic band structure calculations to underestimate the band gap energy has been well documented in previous reports.[62−64] From the projected DOSs (PDOSs) analysis, the bottom of the valence band from approximately −12.5 eV to −10.5 eV is predominantly contributed by nearly equal amount of O-2s and Te-5s orbitals and weakly contributed by P-3sp orbitals. As P-3sp PDOS indicated, the P-3sp orbitals weakly contribute below the E_F which is consistent with the valence bond sum analysis, that is, 4.81 and 4.83 for $P(1)^{5+}$ and $P(2)^{5+}$ cations. As seen in Figure 4a, the top part of the valence band ranging approximately from −2 eV to E_F mainly consists of O-2p in character and the contribution from Te-5sp orbitals is small. Further detailed analyses on the Te-5s and Te-5p with PDOSs reveal that the contribution of Te-5s orbitals is slightly larger than that of Te-5p orbitals in the region. In addition, the Te-5s PDOSs indicate that the major contribution of the Te-5s orbital appears at the bottom of the valence bands, not at the top of the valence band (see Figure 4b).

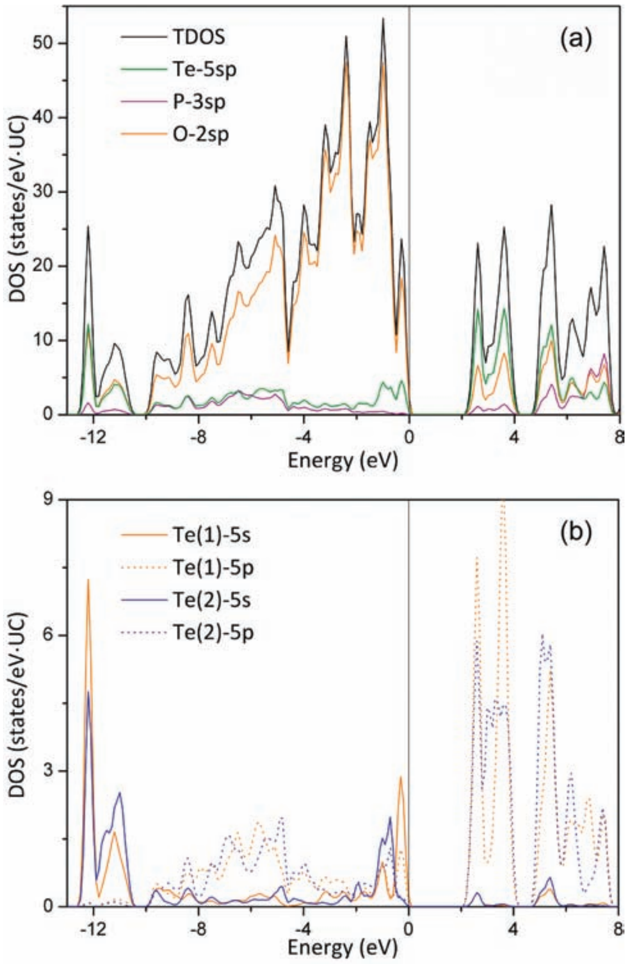

Figure 4. (a) Total and projected density of states (DOS) of $Te_2O(PO_4)_2$ calculated from the pseudopotential method. (b) The detailed PDOS for Te(1) and Te(2). The vertical dotted line at 0 eV indicates E_F.

Figure 5 exhibits bond characters of the bands through crystal orbital Hamilton population (COHP) analyses[65] carried out using the TB-LMTO-ASA method. The −COHP curve for the P−O indicates that the P−O bonds are optimized because the bands showing bonding characters are filled but those of antibonding characters are

---

(62) Eng, H. W.; Barnes, P. W.; Auer, B. M.; Woodward, P. *J. Solid State Chem.* **2003**, *175*, 94.

(63) Mizoguchi, H.; Eng, H. W.; Woodward, P. *Inorg. Chem.* **2004**, *43*, 1667.

(64) Mizoguchi, H.; Woodward, P. *Chem. Mater.* **2004**, *16*, 5233.

(65) Dronskowski, R.; Bloechl, P. E. *J. Phys. Chem.* **1993**, *97*, 8617.

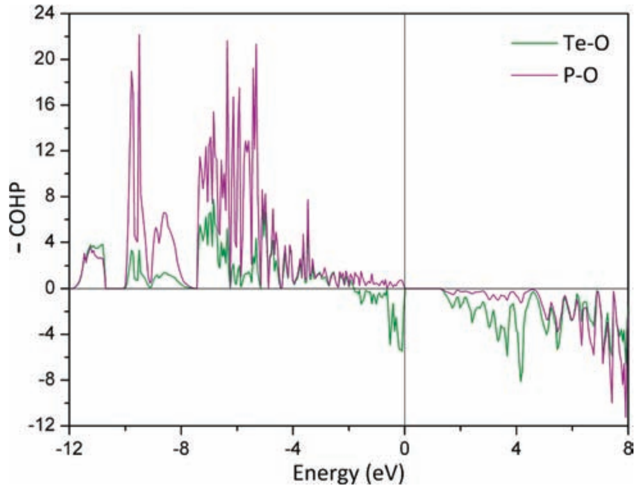

Figure 5. −COHP curves presenting Te−O (green solid line) and P−O (purple) interactions for $Te_2O(PO_4)_2$ calculated using the TB-LMTO-ASA method. The vertical line indicates E_F.

empty. However, the −COHP curve for the Te−O reveals that the bonding and antibonding characters for the Te−O bonds are below and above around −2 eV, respectively. As expected, the Te-5s orbitals near the E_F are directly related to the formation of the stereochemically active lone pairs on the Te^{4+} cations.

From the electronic structure analyses, formation of the stereoactive lone pairs on the Te^{4+} cations is considered to be driven by the cation (Te^{4+})−anion (O^{2-}) interactions[66−68] rather than the intra-5sp mixing of Te^{4+} cations. As shown in Figure 4, the Te-5s orbital is significantly localized at the bottom rather than at the top of the valence band. In fact, an empirical trend with respect to 6s orbital contribution of heavier elements involved in their heavier element oxides such as HgO, Tl_2O_3, PbO, and Bi_2O_3 was observed experimentally and theoretically in regard to a relative contribution of O-2p at the bottom of the valence band.[69] Their O-2p contributions are less than 50% as compared with the contribution of the heavier element 6s orbitals at the bottom of the valence band. We extended the idea to $Te_2O(PO_4)_2$. Likewise, the relative O-2p contribution was estimated calculating a ratio of integrated PDOSs (IPDOSs), that is, IPDOS(O-2p)/[IPDOS(Te-5s)+IPDOS(O-2p)] at the bottom of the valence band (near −13 eV to −10.2 eV). The value is of 0.47 which is close to the value found in Tl_2O_3.[69] Thus, we can deduce that the Te-5s orbital is truly localized at the bottom of the valence band. Therefore, the stereoactive lone pair formation is considered to be driven by indirect 5s-5p mixing of Te^{4+} mediated by O-2p through Te^{4+}−O^{2-} interactions at the top of the valence band. Such interactions may allow forming the stereoactive lone pairs on Te^{4+} cation even at different coordination environments such as $Te^{4+}O_3$, $Te^{4+}O_4$, and $Te^{4+}O_5$.[70]

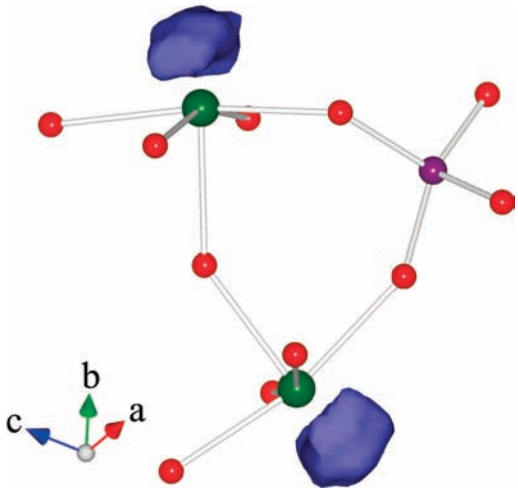

Figure 6. Electron localization function (ELF) isosurface (η = 0.9) of $Te_2O(PO_4)_2$ calculated using the pseudopotential method.

Structure−Property Relationships. As we described in the structure section, $Te_2O(PO_4)_2$ crystallizes in the NCS polar space group *Cc*. It would be important to determine the "net" direction of the lone pair polarizations to understand the origin and magnitude of the NCS properties. We are assuming that the PO_4 tetrahedra do not contribute significantly toward the NCS properties, since the tetrahedra although acentric are not polar as are d^0 transition metal centered oxide octahedra and lone pair polyhedra. For the two unique Te^{4+} cations, each TeO_5 unit has a dipole moment pointing in the direction of the lone pair, although the respective dipole moments do not point directly in any crystallographic direction. While the lone pairs on $Te(1)^{4+}$ approximately point in [011] and [0−11], those on $Te(2)^{4+}$ point in approximate [01−1] and [0−1−1] directions. However, when the all dipole moments are summed, a small net moment is observed pointing approximately in the [001] direction attributable to the slight tilting of the polyhedra (see Figure 2c). It is this small moment that is structurally responsible for the SHG and piezoelectricity of $Te_2O(PO_4)_2$. Our measurements reveal the relatively weak SHG efficiency (50 × α-SiO_2) and piezoelectric response (~20 pm V^{-1}), which is attributable to the lack of greater constructive addition of the local dipole moments.

For visualization of the stereoactive lone pairs, the electron localization function (ELF) calculations[71,72] were performed using the pseudopotential method. Figure 6 shows ELF visualization with η = 0.9 for $Te_2O(PO_4)_2$. As anticipated, highly asymmetric lobelike isosurfaces are found near the Te^{4+} that may be considered as a stereoactive lone pair. As described earlier, the stereoactive lone pairs are not aligned oppositely; thus, their local dipole moments are not canceled out. In other words, the NCS functional properties of $Te_2O(PO_4)_2$ are dominantly dependent on the distortion and polarization associated with the Te^{4+} cations.

To better understand structure−property relationships as well as the asymmetric coordination environment of

---

(66) Lefebvre, I.; Szymanski, M. A.; Olivier-Fourcade, J.; Jumas, J. C. *Phys. Rev. B.* **1998**, *58*, 1896.

(67) Watson, G. W.; Parker, S. C. *J. Phys. Chem. B* **1999**, *103*, 1258.

(68) Watson, G. W.; Parker, S. C.; Kresse, G. *Phys. Rev. B* **1999**, *59*, 8481.

(69) Payne, D. J.; Egdell, R. G.; Walsh, A.; Watson, G. W.; Guo, J.; Glans, P. A.; Learmonth, T.; Smith, K. E. *Phys. Rev. Lett.* **2006**, *96*, 157403/1.

(70) Kim, J.-H.; Halasyamani, P. S. *J. Solid State Chem.* **2008**, *181*, 2108.

(71) Becke, A. D.; Edgecombe, K. E. *J. Chem. Phys.* **1990**, *92*, 5397.

(72) Savin, A.; Jepsen, O.; Flad, J.; Andersen, O. K.; Preuss, H.; Von Schnering, H. G. *Angew. Chem., Int. Ed.* **1992**, *31*, 187.

Te^{4+}, we also calculated the local dipole moment for $Te_2O(PO_4)_2$. This approach has been described earlier with respect to metal oxy-fluoride octahedra.[73,74] We recently reported the dipole moments for TeO_5.[7] An examination of 30 examples of TeO_5 polyhedra revealed that the dipole moments range from 4.31 to 10.82 D (D = Debyes). Similarly, we found that the local dipole moments for the two unique TeO_5 polyhedra, $Te(1)O_5$ and $Te(2)O_5$ in $Te_2O(PO_4)_2$ are about 6.09 and 6.53 D, respectively.

Conclusion

We have successfully synthesized a new NCS tellurite phosphate material, $Te_2O(PO_4)_2$, through a standard solid-state reaction. $Te_2O(PO_4)_2$ has a novel three-dimensional framework structure with Te_2O_9 dimers and PO_4 tetrahedra. Infrared and UV−vis diffuse reflectance spectroscopy, thermogravimetric analysis, and electronic structure calculations have been performed on the reported material. Powder SHG and piezoelectric measurements showed that the material has a SHG efficiency of $50 \times \alpha\text{-SiO}_2$ and $d_{33} = 20$ pm V^{-1}, respectively.

Acknowledgment. This research was supported by Basic Science Research Program through the National Research Foundation of Korea (NRF) funded by Ministry of Education, Science & Technology (Grant 2010-0002480). S.-H.K., H.-Y.C., and P.S.H. thank the Robert A. Welch Foundation (Grant E-1457), the ACS PRF 47345-AC10, and the NSF (DMR-0652150) for support.

Supporting Information Available: X-ray crystallographic file for $Te_2O(PO_4)_2$ in CIF format, calculated and observed X-ray diffraction patterns, thermogravimetric analysis diagram, UV−vis diffuse reflectance spectrum, phase-matching curve, and displacement vs electric field loop for $Te_2O(PO_4)_2$. This material is available free of charge via the Internet at http://pubs.acs.org.

---

(73) Maggard, P. A.; Nault, T. S.; Stern, C. L.; Poeppelmeier, K. R. *J. Solid State Chem.* **2003**, *175*, 25.

(74) Izumi, H. K.; Kirsch, J. E.; Stern, C. L.; Poeppelmeier, K. R. *Inorg. Chem.* **2005**, *44*, 884.